A REVIEW OF HYPERSONIC BOUNDARY LAYER STABILITY EXPERIMENTS IN A QUIET MACH 6 WIND TUNNEL

Stephen P. Wilkinson*
NASA Langley Research Center, Hampton, Virginia 23681-0001

Abstract

Three recent experimental studies of transition on cones with adverse pressure gradient produced by a flared afterbody and with the additive stability modifiers of wall cooling, angle of attack and bluntness are reviewed. All test were conducted in a quiet Mach 6 wind tunnel. The dominant instability was found to be the second mode. For the cases examined with linear stability theory, the N factors at mode saturation were in the range of 8.5 to 11. Evidence of a combined second-mode/Görtler transition process was found. Mean, rms and spectral freestream data for the quiet facility is presented and the role of low frequency freestream noise is discussed.

Introduction

One of NASA Langley's primary roles in the National Aerospace Plane (NASP) venture of the 1980's and early 1990's was to develop a collection of low free-stream-disturbance, hypersonic wind tunnels covering Mach numbers from 6 to 18. These tunnels were to be used to obtain important experimental instability and transition data required to validate computations and theory for various stability modifiers such as curvature, bluntness, heat transfer and angle of attack. When the NASP project ended, some of the facilities developed in that era continued to operate. Two of these were the NASA Langley Mach 6 Quiet Nozzle in the Nozzle Test Chamber (M6NTC) and the 18 Inch Mach 8 Quiet Tunnel (18M8QT). The 18M8QT facility was a modification to an existing conventional blow down facility to allow quiet tunnel operation and was reported on earlier[1,2]. It is currently undergoing shakedown testing and flow quality measurements are not yet available. This paper, therefore, deals exclusively with the M6NTC facility and recent stability experiments that were conducted in it.

The M6NTC studies are basically a study of the second mode instability and its sensitivity to various geometrical and boundary condition stability modifiers. A comprehensive review of the second mode is not presented here, however, studies with particular relevance to the current work are cited. A good historical review of second mode studies is contained in the introduction to Stetson and Kimmel's[3] review of hypersonic transition. That paper goes on to review a series of experimental instability and transition studies conducted at Mach 8 in the Arnold Engineering and Development Center (AEDC), Von Karman Facilites Tunnel B that provide the closest comparison data for the current studies. Since all of the current work is conducted with a streamwise, adverse pressure gradient, the studies by Kimmel[4] on hypersonic transition zone lengths under pressure gradient and Malik, Balakumar and Chang's[5] computational study of those models are relevant. The former work was an experimental investigation of transition zone lengths at Mach 8 in AEDC Tunnel B on a parametric series of cones with ogive and flare afterbodies. The models studied in the current Mach 6 work were similar to Kimmel's largest adverse

* Aerospace Engineer, Experimental Methods Branch, Senior Member AIAA

pressure gradient case. Reference 5 reports on mean flow computations and stability analyses showing the destabilizing influence of adverse pressure gradient for two of the cases of reference 4. The current work relies heavily on linear stability theory as a basis of comparison, in particular, on the linear stability theory e^N tools developed by Malik[6]. All of the current models were studied with the e^N method and those computations are contained in a report by Balakumar and Malik[7]. For guidance on the physical processes involved in the transition zone, the combined parabolized stability equation (PSE) and direct numerical simulation (DNS) solutions by Pruett and Chang[8] based on the AEDC Mach 8 cone experiments are very helpful. That work is an in-depth analysis of hypersonic transition and shows that interaction of oblique rope-like structures or vortices associated with the the second mode is the most likely path to transition.

Before presenting the M6NTC experiments, a brief discussion of the technical and programmatic environment in which the work was conducted is useful since these issues had a direct impact on both the course of the work and key decisions regarding experimental protocol. The M6NTC was successfully developed[1,9] and heralded as the first hypersonic quiet tunnel capable of high Reynolds number performance. There was a problem, however, in that its quiet flow performance in the upper half of its operating range turned out to be erratic and an extended period of study to develop corrective measures was required. In the same time frame, NASP was discontinued and NASA found itself in the midst of organizational restructuring. The M6NTC survived as an important but relatively low-cost, work-in-progress facility. The end-of-an-era was clearly at hand however with the announcement that Nozzle Test Chamber was to be physically relocated and given on a new mission that did not include quiet flow operation. This was necessary in order to make way for expanding operations of the Langley 20 Inch Mach 6 tunnel, an important NASP facility in its own right, that shared the same room. In this environment, it was decided that the final program for the M6NTC prior to its decommissioning, a period of approximately 14 months, would be to acquire as much instability and transition data as possible using the models and tools on hand.

Prior to testing, the erratic transition behavior on the Mach 6 nozzle's wall had to be dealt with. As discussed in reference 1, the problem was attributed to either deposition of atmospheric dust on the nozzle throat surface or surface oxidation. Summarizing reference 1, both possibilities were treated - the dust with better filtering and the oxidation with a new nickel-phosphorus alloy surface coating. The end result was that the surface coating apparently added a small amount of waviness that degraded nozzle performance. The nozzle was now limited to a lower but stable unit Reynolds number quiet flow capability of approximately 3 $x10^6$/ft. While the shortcomings of the attempted repair were disconcerting, the nozzle still had impressive laminar flow capability and was considered suitable for continued study.

NASP was seriously lacking experimental hypersonic instability and transition data obtained in a low disturbance freestream environment. This was especially evident in the very basic case of adverse pressure gradient. Since adverse pressure gradient promotes earlier transition and since several adverse-pressure-gradient, conical models had previously been fabricated

for NASP for use in the M6NTC, the decision was made to base the final activities in the M6NTC on detailed studies of these existing adverse pressure gradient models along with a new and improved mapping of the nozzle's flow quality. The lower quiet flow Reynolds number requirement of an adverse pressure gradient model was well suited to the reduced quiet flow capability of the M6NTC. Additional funding was secured to add a cold-wall companion model to extend the stability modifier data base.

Since Langley had not previously conducted detailed stability experiments (as distinct from transition location experiments) in any of its hypersonic facilities, the tools and procedures for doing so had to be developed. Training of new personnel to conduct the work was also required. In the end, the effort seems to have been worthwhile. While, as will be shown, the data are not without interpretive issues and the fashion in which certain diagnostics were implemented (particularly the hot wire) may be subject to debate, a unique data base was acquired under low disturbance, hypersonic conditions.

What follows is a review of four, previously published studies conducted in the M6NTC in its final months of service. The first study by Blanchard, Lachowicz and Wilkinson[10,11] measured the flow quality in the M6NTC after the nozzle plating modification discussed above. Mean flow (pitot pressure) and rms fluctuation maps (hot wire) were obtained in the flow region occupied by the models. It lacks spectral data which was included, however, in each of the subsequent studies of the various models.

The second work by Lachowicz, Chokani and Wilkinson[12] (see also references 13, 14, 15) examined the stability of flow over a sharp-tipped conical body consisting of an initial five-degree half-angle cone followed by a tangent, circular, flare used to generate an adverse pressure gradient. The experimental data include calibrated mean and dynamic boundary layer profiles, equilibrium wall temperature, and wall pressure at zero angle of attack along with data corresponding to small nose radii bluntness. CFD computations of the mean flow were also included.

The third work by Doggett, Chokani and Wilkinson[16] (see also references 17, 18 and 19) extends the work of Lachowicz to include angle-of-attack. Angles of 0, 2 and 4 degrees are examined. Data include mean and fluctuation data and companion CFD mean flow computations. Bispectral analysis of the fluctuation data is included.

The fourth and final work by Blanchard[20] (see also reference 21) deals with wall cooling of a similar adverse pressure gradient model used in the prior studies. Uncalibrated mean flow and fluctuation hot wire data are presented.

The motivation for this review revolves around two related questions. The first is to what extent was our knowledge of hypersonic transition enhanced by the studies introduced above; the second question is what differences from conventional tunnel testing can be attributed to the low disturbance environment. With regard to the second question, there is not a one-to-one correspondence between quiet and conventional tunnel data. The closest comparison data is the serial work of Stetson, Kimmel and their co-workers as reviewed in reference 3 and the later pressure gradient work of reference 4. The M6NTC, as in other Langley low disturbance tunnels, employs a bleed slot upstream of the nozzle to help maintain

laminar flow on the nozzle wall downstream. By closing the exit valve from the bleed slot, flow spills over the bleed lip and trips the flow creating a noisy free stream environment not unlike that see in conventional tunnels. For the M6NTC, such an operation universally had an overpowering effect on both the nozzle and model boundary layer transition processes, presumably through a high intensity bypass mechanism. This brute-force tripping technique was, therefore, not used routinely. A more desirable input would be better differentiated in terms of frequency, wave propagation angle and amplitude in order to examine receptivity issues. Such is not the case in these experiments and the role of free stream disturbances will continue to be a matter of inference and to some extent speculation until more controlled environments or experiments become available. For example, an experiment is currently underway[22] at Langley using glow discharge actuators to introduce controlled disturbances into the boundary layer of a seven degree cone at Mach 3.5.

Facility Characteristics

The M6NTC is a small open-jet, blowdown apparatus with a 39.76 inch long, axisymmetric nozzle (throat minimum to exit) and a 3.746 inch exit radius. The usual operating stagnation temperature was in the range of 350 - 400 deg. F and the flow was quiet up to a stagnation pressure of 130 psia (Re = 2.8 $x10^6$/ft) although distinctive noise patterns in the aft portion of the nozzle were observed even at this pressure as discussed below. The tunnel did not have a model injection system and the facility was pre-heated and tests run with the models in place. The facility could be run almost continuously due to the massive air supply and vacuum systems to which it was connected but the run time was typically limited to 30-60 minutes. Figure 1 shows the overall layout of the facility and Figure 2 a few relevant details of the nozzle and model placement.

The free stream flow measurements conducted by Blanchard (reference 10) represented a major improvement in both in detail and understanding of the Mach 6 nozzle flow. These measurements were carried out after the nozzle re-plating procedure discussed in the introduction and take precedence over the measurements reported on in reference 9. Figure 3 shows a Mach number contour map (based on pitot tube pressure measurements) in a horizontal plane coincident with the nozzle centerline. As shown there is a large region of nearly uniform flow. The average Mach number is 5.91. There is a one percent overshoot in Mach number on the centerline near X= 25 inch. This overshoot was attributed to the nozzle re-plating procedure and was not observed in the original nozzle design or early measurements prior to the re-plating.

Early assessment of the free stream flow quality was based either on the rms hot-wire fluctuation distribution on the nozzle centerline (reference 9) or, in later studies on the turbulent burst intermittency (reference 2) . For the latter, time records of hot wire output voltage fluctuations show an absence of high intensity intermittency up to a stagnation pressure of 130 psia (see Figure 1 in reference 2). As pressure is increased, intermittency develops until the flow becomes completely turbulent somewhere in the region of 200 psia. The flow up to 130 psia was termed "quiet" and flow at higher pressures "noisy", i.e. quiet flow was implicitly defined as the absence of measureable hot wire intermittency. Figure 4 (from reference 10) shows contours of constant rms anemometer output (uncalibrated, constant overheat) in the aft region of the nozzle. The striking feature of the plot is the inclined contours,

presumably due to low level, convecting disturbances from the nozzle wall, propagating into the free stream. Figure 4 adds a new dimension to the study of freestream noise by showing that in the pre-intermittency region, a pattern of noise is evident. A new, finer definition of quiet flow now becomes the absence of convective noise patterns in the contour plot. Eventually the signal becomes lost in the noise floor of the anemometer and recording devices making it difficult to determine with certainty the upstream location where the pattern starts.

There is a clear Reynolds number dependency to the rms contours shown in Figure 4. Figure 5 shows a compilation of streamwise slices through the six contour plots on the nozzle centerline for a range of unit Reynolds numbers. The abscissa is the length Reynolds number based axial distance from the throat to the hot-wire probe. Figure 6 shows the same data replotted based on a virtual origin of the fluctuations 14.76 inches downstream of the nozzle throat. These replotted data to collapse into a single curve. This finding suggests that transition on the nozzle wall is due to an orderly growth process, presumably the Görtler mode on the concave regions of the nozzle wall. The Reynolds number dependency shown in Figure 6 was also previously noted in the initial studies of the Mach 6 nozzle as reported in reference 9. In that study (prior to the nozzle replating), a Reynolds number dependency similar to that shown in Figures 4 and 5 was observed based on centerline rms readings alone up to a stagnation pressure of 225 psia. Above 225 psia, a by-pass mechanism appeared to take over, causing the entire region of accessible flow to transition to turbulence. Intermittency measurements were not reported in reference 9.

The implication of these freestream noise measurements to subsequent model instability measurements is that a criteria of quiet flow based on the absence of intermittency does not capture all of the noise features of the free stream flow. In general, for the models discussed in this paper, any hot wire signals in the receptivity-sensitive locations (the model nose and cone-flare regions) would have been masked by the electronic noise floor of the anemometer and recording devices. The aft portions of the model (where exponentially growing second mode disturbances were observed) experienced the low level, growing noise patterns observed in Figures 4 through 6 and previously in reference 9.

For stability measurements on models, knowledge the full three-dimensional wavenumber spectrum would be the ideal input condition. With a single hot wire, however, only scalar frequency spectra are available. Frequency spectra are not reported in reference 10, however, they are included in the reports on the model experiments (i.e. references 12, 16, 20 and thier companion documents) and are discussed later in the context of the models. In general, what the spectral data show is a low frequency band peaking at 0 Hz rolling off to the electronic noise floor of the unstrumentation at somewhat less than 100 kHz. There were no detectable disturbances with the current instrumentation at the dominant second mode frequencies (~250-300kHz) however this is not to say that they were not present. The low frequency band is most likely related to the rms contours shown in Figure 4 giving a clue to their origin. It is known that the dominant transition mode for the nozzle wall is Görtler vortices (reference 9) and some of the low frequency disturbances are likely due to sporadic development and meandering of the vortices. Other low frequency sources would include

unsteady Mach waves from small nozzle waviness and acoustic disturbances from the settling chamber.

Model Stability Experiments

As discussed in the introduction, three separate experiments were conducted using a variety of stability modifiers on a similar base configuration. For brevity, for the remainder of the paper these works will be denoted by the first author: Lachowicz for the adiabatic, flared cone with bluntness (reference 12 and its companion documents references 13,14 and 15); Doggett for the adiabatic flared cone at angle of attack (reference 16 and its companion documents 17, 18 and 19); and Blanchard for the cold-wall flared cone (references 20 and 21). Lachowicz and Doggett used the same physical model with a 10 inch right-circular, 5 degree half-angle cone preceding a tangent-flare with a radius of 93.071 inch. The total model length was 20 inches. The model is denoted 93-10 referring respectively to the approximate radius of the circular flare arc and the location of the tangency point. Blanchard used a different model with a six inch 5 degree half-angle cone preceding a 91.44 inch flare. The total model length was 18 inches. It is denoted model 91-6. Further details are found in the original documents.

The common feature of all of the models and experiments was the tangent, circular-arc flare used to produce the adverse pressure gradient. This was a much simpler configuration that the power law used for the models in reference 4 but as will be shown produced a nearly linear pressure gradient. Unlike reference 4, however, there was a discontinuity in the curvature at the point of tangency. Another feature of the models is that from an analysis point of view, the effects of bluntness, angle-of-attack and wall cooling must be separated from the adverse pressure effects. Without the adverse pressure gradient, however, transition would not have been attained within the limited quiet flow Reynolds number range of the facility which was the overriding consideration. As will be shown the additive effects are not subtle and analysis using linear stability, PSE or DNS tools should be just as enlightening as proceeding from a base zero-pressure-gradient case.

Both of the models tested in this series of investigations were previously studied by Balakumar and Malik[6]. Using a Navier-Stokes code to compute the mean flow and linear stability theory N-factor analysis to determine the stability of the flow, reference 6 provides a rich data base for comparison with the current data. Another source of computed comparison data, although less direct, are PSE/DNS solutions of Pruett and Chang[8] for transition on a right circular cone at Mach 8 corresponding to the work of Stetson (ref. 3). A very recent work by Pruett and Chang[23] computes the flow over model 93-10 and deals specifically with effects of the adverse pressure gradient. Since that document is in review as of this writing, only limited references to it can be made.

Hot Wire Diagnostics

Before dealing with the details of the model experiments, discussion of the primary diagnostic tool, the hot wire anemometer is required. All of the experiments shared basically the same diagnostic techniques with some upgrading of equipment between tests. One of the most troublesome features of conducting low level electronic flow measurements in the Langley Hypersonic Facility Complex (the location of the

Nozzle Test Chamber) is electromagnetic interference (emi). While techniques exist for shielding or guarding instruments from emi, the hot wire is unique in that the probe must remain exposed in order to function. The major source of emi in the building has been identified as the multi-megawatt electric heater controllers used to heat the flow supplied to the hypersonic tunnels. While this noise tends to be narrow band and centered around 40-50 kHz, its amplitude can be an order of magnitude greater than the signal under investigation thereby masking the low level signals. Not all anemometers respond equally to emi. Early in the current investigations, a commercial constant current anemometer (CCA) system was tried and emi pickup was unacceptably large. The same was true of a commonly used, commercial constant temperature anemometer (CTA). A new, proprietary anemometer system, however, called the "Constant Voltage Anemometer" (CVA) under development through Langley at that time[24,25,26,27] was surprisingly immune to the same emi picked up by the other instruments for reasons that have not yet been investigated. The CVA had been reasonably well analyzed and studied but there were still gaps in understanding regarding frequency response and calibration. The dilemma for the researcher was whether to use the well qualified CCA or CTA techniques with the potential loss of important information in the high amplitude noise band or to go with the new, incompletely studied CVA that showed better noise immunity. There were also issues of limited test time complicating the situation. In the end, the clarity of the low level signals won out and the CVA was adopted as the dynamic measurement system for all of the Mach 6 experiments reported on in this review.

The major drawback of the CVA was that it lacked extensive calibration studies and the frequency compensation for the sensor was fixed at constant value for most tests. For a fixed wire voltage, the wire overheat varies through the hypersonic boundary layer due to the total temperature profile. Also, the quoted frequency response of the CVA of 350kHz was based not on actual sensor response but rather on proprietary features of the circuits and broad-band noise response. The basic CVA algorithm at that time did not permit square-wave setting of the frequency response. For the Lachowicz study, a simple calibration for mass flux and total temperature for the hot wire was used. For Doggett, Blanchard and the M6NTC facility study discussed earlier, the data are uncalibrated hot wire outputs. In certain cases, the data were acquired at constant hot wire overheat rather than constant wire voltage. While the difference was not large and did not change any conclusions, the reader is cautioned to refer to the original documents to determine how the CVA was used in a particular situation before drawing conclusions that may depend on frequency response or calibration. In general, frequency data is safe; amplitude data must be interpreted with more care.

Adiabatic Flow Over a Flared Cone

Lachowicz presents data taken on model 93-10 at nominally zero angle of attack with a sharp tip and three cases of small nose radii bluntness. The major findings pertain to the model's wall temperature distribution under the transition process, dynamic hot-wire measurements in the transitioning boundary layer and the pressure distribution. First, however, it is important to examine the spectra of free stream disturbances to which the model was exposed.

Figures 7 and 8 show plots of the normalized hot wire output spectra for a probe in the free stream at plus and minus 1.25 and 2.25 inches off the nozzle centerline. The data was acquired at a fixed unit Reynolds number and the probe position was varied. The Reynolds number Re_{X_n} is based freestream conditions and distance from the nozzle throat minimum radius location (X=0). The data clearly show a growing low frequency disturbance field consistent with the rms fluctuation contour map in Figure 4. The contour labeled "0.030" in Figure 4, representative of the beginning of the radiated low frequency noise region, intersected the 93-10 model at roughly 13 inches from the sharp nose tip. Therefore all of the right circular cone and the first 3 inches of the flare were in a freestream without disturbances above the anemometer noise floor. As will be shown, this low frequency band is low relative to the dominant second mode which falls in the 250 to 310 kHz range. The curves merge with the electronic noise in the 100-150kHz range, therefore higher frequencies are not shown. The key findings are that there are no measurable fluctuations above the electronic noise level in the second mode frequency range or from the low frequency facility noise on the first two thirds of the model.

Figure 9 shows the wall temperature distribution for the sharp-tipped case as determined from a ray of thermocouples attached to the backside of the thin-walled surface. The model was run at constant flow conditions long enough to reach approximate thermal equilibrium. There are three significant features displayed in Figure 9: 1) the excellent correspondence between the measured and theoretical data in the pre-transitional region of the model; 2) the abrupt departure from the laminar flow solution on the aft portion of the model that is indicative of transition; and 3) the dramatic change in the temperature distribution when the tunnel flow is intentionally made noisy. This was done by closing the bleed valves that remove the settling chamber wall boundary layer upstream of the nozzle's throat thereby tripping the nozzle wall boundary layer. The difference between the quiet and noisy flow data are ample proof of the value and necessity of low-disturbance facilities for transition research.

The more abrupt nature of transition in the quiet flow case than in the noisy case affects the measurement of the transition zone length. Kimmel[4] has examined transition zone lengths in AEDC Tunnel B, a conventional facility, for both favorable and adverse pressure gradients and reports that the later results are inconclusive. Given the difference between the noisy and quiet flow cases in Figure 9, however, it is apparent the facility noise can have a major impact on the transition zone length measurements. As indicated earlier, the current facility is probably atypical in its noisy mode due to the large effective boundary layer trip formed by the inactive bleed slot upstream of the throat. Nonetheless, the implication is clear that noisy freestream flow can stretch out the observed transition zone.

Figure 10 is a plot of the normalized hot wire output spectra take at the maximum energy height in the boundary layer at each streamwise measurement station for the sharp tipped case. The data were acquired at constant unit Reynolds number. The dominant mode is the peak at approximately 226 kHz corresponding to a linear stability theory prediction of 230kHz[7] for the second mode. There is also growth in the low frequency region between 0 and 100 kHz and at the second mode harmonics of 449kHz and

670 kHz. The low frequency growth is the same discussed in reference to Figures 7 and 8. More extensive data on this region was obtained for model 91-6 (both adiabatic and cold wall) and it is shown in reference 20 (also reference 21) that the low frequency forced disturbances are larger and grow faster in the boundary layer than in the free stream. These results appear to be consistent with the phenomenon of sound forcing of supersonic laminar boundary layers as developed by Mack[28] and studied by Kendall[29] (See additional discussion in the next section on the cold wall experiment.)

The two harmonics shown in Figure 10 are not predicted by linear theory. When the Navier-Stokes equations are linearized, terms containing products of fluctuations are discarded, however, it is precisely these product terms that produce the harmonic frequencies. Appearance of the harmonics is therefore associated with non-linearities. With regard to the harmonics, it should be pointed out that frequency response of the CVA anemometer was quoted by the vendor as approximately 350 kHz. The harmonics at 449 and 670 kHz are clearly in the roll-off band of the instrument and some attenuation has occurred. The growth rate at a fixed frequency in the roll-off region, however, would remain valid.

In reference 7, the integrated growth factors (N-factors) for the 93-10 model (adiabatic) and model 91-6 (adiabatic and cold wall) were computed and can be compared to experimental data. Figure 11 is a composite of all N-factor data for both models. Exploiting the linearity of the solutions, the experimental data is shifted at constant Re_x to match the computations. The degree of fidelity between the slopes of the experimental and computational data is surprisingly good over the central, linear portion of each curve. At the low end, the data merge with the electronic noise floor and at the high end, non-linearities and turbulent breakdown set in. This is a dramatic example of the power of linear stability theory to predict a large portion of the instability process when the proper physics are included in the computations and the data is obtained in a suitably low-disturbance environment. With regard to the freestream spectra, it was noted that there were no detectable fluctuations in the frequency band of the second mode. The question therefore arises as to how the observed disturbances are initiated. From Figure 11 is clear that the electronic noise floor is 2 to 3 orders of magnitude too high to resolve fluctuations in the vicinity of the neutral curve. Until significant improvements in signal-to-noise ratio are available, the nature of the "natural" seeding for the second mode will remain an open question.

Lachowicz also examined the effect of small nose radii bluntness on transition. Figure 12 shows the equilibrium wall temperature distributions for the sharp-tipped case and three nose radii. In all cases, the small bluntness was stabilizing. In the case of the 1/32 inch nose radius, growth of the second mode around 230 kHz was observed. For the 1/16 inch and 1/8 inch cases, no evidence of the second mode was observed. Further details are found in references 14 or 15 (identical documents).

Flow over a Flared Cone with Wall Cooling

Blanchard examines the stability of boundary layer flow over a cone similar to that used in Lachowicz but designed with provisions for cold wall operation. The right circular cone portion was 4 inches shorter that the 93-10 model and

had a 3 inch shorter flare arc radius. The aim was to develop a slightly greater pressure gradient than in the 93-10 case and apply the pressure gradient to a greater extent of the model. Internally, the model was basically a parallel heat exchanger with coolant entering along a passage in a central core body on the streamwise axis, reversing direction just downstream of the 1.5 inch long, screw-in nose tip and flowing out through an annular passage between the model skin and the core body. The tip region of the cone was uncooled. The model was instrumented with a ray of thermocouples and a surface pressure ports as in the case of the 93-10 model.

The effects of wall cooling on hypersonic transition are reasonably well understood. Linear stability theory shows that the second mode frequency increases due to the thinned boundary layer and the growth rate increases resulting in a lower transition Reynolds number. Tests in the M6NTC confirm these trends and show agreement with linear stability theory. Since all tests were conducted in the same facility at the same unit Reynolds number (the maximum quiet flow unit Reynolds number for the facility), the free stream spectra shown in Figures 7 and 8 are valid for this test as well. Blanchard, however, provided additional free stream data by conducting a streamwise survey of the model in the region between the boundary layer edge and the model's shock. This is shown in Figure 13. The data show the same low frequency growth discussed earlier, but nothing in the second mode frequency range or other regions above the noise floor out to the bandwidth of the anemometer. The contour labeled "0.030" in Figure 4, representative of the beginning of the radiated low frequency noise from the nozzle wall, intersected the 91-6 model again at roughly 13 inches from the sharp nose tip as in the case of the 93-10 model. Therefore, more than two-thirds of the model were in a freestream without measurable low frequency facility noise.

The wall temperature is a critical experimental variable required for computation of the mean flow and stability. Figure 14 shows the equilibrium wall temperature measured with thermocouples embedded in the thin wall of the model. The effect of the uncooled tip is evident as well as the abrupt change in temperature associated with transition. To test the boundary layer thinning action of the cold wall, estimates of the boundary layer thickness were made by traversing an unheated hot wire through the boundary layer and monitoring both the change in resistance due to the local total temperature and the mean CVA output voltage. Both measurements yielded similar results. This method was able to validate mean flow computations of reference 7 as shown in Figures 15 and 16. The deviation of the measured data for X>14 inch is due to transition.

Spectra taken following the maximum fluctuation amplitude height in the boundary layer are shown in Figures 17 through 20 displayed in alternate perspective and frontal view formats. As shown in Figures 17 and 18, there is a dominant second mode band with peaks at 275kHz and 291kHz for the adiabatic wall case and in Figures 19 and 20 for the cold wall case, a similar band centered at 306 kHz with side peaks at 291 and 320 kHz. Corresponding linear stability results from reference 7 are 270kHz for the adiabatic wall case and 310 for the cold wall case. In the cold wall case computations, a constant wall temperature of 420 degrees R was assumed whereas the experimental case was non-uniform and about 50 degrees R higher. The cause of the double and triple peaks in the second mode bands in not known. It is noted however that the there

is a consistent difference between the peaks of approximately 15kHz which corresponds to a dominate frequency in the low frequency region attributed to facility noise. Bispectral data for model 93-10, presented in references 18 and 19, however, shows no coupling between the facility noise and the second mode and the issue remains unresolved. In any case, given the differences between the theoretical assumptions and the actual experiment, linear stability theory is shown to be particularly good at predicting the most amplified disturbance frequency. The integrated growth rates have already been presented in Figure 11 showing excellent agreement with theory.

An interesting result of the flared cone experiments that was captured particularly well in the Blanchard experiments is the shape of the rms fluctuation profile normal to the wall. For the case of a right circular cone, in the AEDC Mach 8 experiments (see figure 5 in reference 3) this shape consisted of a single peak at the generalized inflection point near the boundary layer edge. With the application of streamwise concave curvature (adverse pressure gradient), however, the profile is altered and appears to take on a double peaked structure as shown in Figures 21 and 22 for the adiabatic wall case and 23 and 24 for the cold wall case. Figure 21 and 23 are contour plots of constant natural log rms fluctuation amplitude and Figure 22 and 24, plots of the same data at a fixed streamwise location at the upstream edge of the measurement domain. The hot wire data are uncalibrated and recorded at constant CVA wire voltage. At first there was suspicion that the observed double peak might be an artifact of rapid changes in wire sensitivity and large variations in T_o and density through the boundary layer. Figure 25 however (unpublished data provided courtesy of P. Balakumar from the data base of reference 7) also shows a double peaked eigenfunction albeit with the lower peak closer to the wall and an overall greater Y extent. A preliminary look at a forthcoming DNS and PSE computations for the Lachowicz experiments in reference 23 also show a qualitatively similar double peaked eigenfunction for Model 93-10. The data in Figure 22 are therefore at least consistent with theory and may be real rather hot wire calibration artifacts. Regarding the possible cause of the double peaked eigenfunction, reference 23 also looks at the growth of the Görtler mode. Velocity and temperature eigenfunctions for the Görtler mode ((0,1) harmonic in reference 23) show the double peak which suggests that a second-mode/Görtler interaction may be operative. The maximum Görtler number, N_G, for the 93-10 model, however, was approximatley 3 based on reference 23 boundary layer momentum thickness computations. Model 91-6 was not significantly different so a similar value would be expected. This value is less than one half of the value normally associated with breakdown of the Görtler mode (N_G=7) in low speed flows, although even at this level, it may still be sufficient to cause a measureable effect on the eigenfunction. Whether the double peaked eigenfunctions are sufficient evidence of Görtler vortices or a mixed-mode transition process (Görtler and second mode) is not entirely clear. Data is presented in reference 23 for the Görtler mode growth rate on model 93-10. It has been pointed out that the Görtler growth rate is nearly as large as that of the dominat second mode (C.-L. Chang, private communication). This would suggest that the Görtler is not an insignificant player and that the double-peaked eigenfunction may be evidence of its existence.

Another interesting feature of the eigenfunction plots (Figures 21-24) is that they take on the well developed, double-peaked form before measurable spectral growth occurs. From Comparing, say, Figures 17 and 21 for the adiabatic wall case, the spectral peak at second mode frequency (Figure 17) is just beginning to grow at about X=9 inch whereas the eigenfunction (Figure 21) appears to be fully formed at that same location and presumably some distance upstream as well. There is clearly disturbance mode development upstream of X=9 inch on the model which is not unexpected in consideration of the N-factor distribution shown in Figure 11. Better than one half of the linear theory growth region is both inaccessible by the hot wire and below the noise floor of the anemometer. It is still somewhat puzzling however as to why the eigenfunction plots seems to pick up the growth better than the spectral plots.

Another question involves the role of the low frequency forcing discussed in relation to Figures 4-6 on the eigenfunction and spectral development. Figure 26 shows the growth of disturbances at a representative low frequency of 15 kHz both in the model boundary layer and in the freestream. Disturbance growth rates greater than the freestream are observed in accordance with Mack's forcing theory[28]. It is clear therefore that a fluctuation component other than the second mode is present and that the additional component is facility-dependent. The streamwise location where the 15kHz disturbance begins to grow is consistent with the radiated noise pattern of Figure 4. The implication appears to be that the forced growth is too weak and at too low a frequency to significantly alter the dominant second mode dynamics.

Flow over a Flared Cone at Angle of Attack

The third stability modifier applied to the flared cone configuration was angle of attack. Doggett conducted experiments with the sharp tipped 93-10 model (the same one used by Lachowicz) placing it at angles of attack of 0, 2 and 4 degrees and measuring equilibrium wall temperature, pressure distribution and the mean and dynamic boundary layer flow for each case. The significant findings of this investigation were consistent with earlier findings in conventional facilities (e.g. reference 3 and citations therein). As the model is pitched, boundary layer flow on the windward ray is stabilized and flow on the leeward ray destabilized. Figure 27 (Figure 3.67 from reference 18) is a partial stability diagram for the angle of attack studies based on experimentally determined growth rates. The contours are in the range of growth rates $-\alpha_i$=4 to 9 x10^{-3} and were chosen to highlight the maximum amplification points of the dominant instabilities. The neutral stability curves could not be determined since they were significantly below the anemometer noise level. The plot summarizes most of the significant findings. For the zero degree baseline case, the second mode at about 266 kHz is dominant. At 2 degree angle of attack on the windward ray, the dominant frequency increases and the maximum amplification region moves downstream. On the leeward ray, frequencies decrease and the maximum amplification region shifts forward.

Navier-Stokes mean flow computations of the flow in Doggett make it possible to estimate the second mode frequency from the ratio of the boundary layer mean velocity at the generalized inflection point and twice the boundary layer thickness. The estimated second mode frequency agrees well with the measured frequency

of the second mode peaks for the 0 and 2 degree windward cases. (See Figures 6b and 7b in reference 16). In the 2 degree leeward case the measured second mode cannot be clearly distinguished due to the extensive breakdown of the flow and presence of low frequency facility noise. However, the localized contour peaks at 140kHz are beyond the predicted second mode frequency. In the leeward case, the cross flow instability mechanism is expected to play an important role and may likely be associated with these peaks. Additional measurements are required to verify this observation.

Doggett also performed bispectral analysis of the boundary layer disturbances and schlieren flow visualization of the boundary layer on the aft (visible) portion of the model. The bispectral analysis showed deterministic phase coupling between the dominant second mode frequency and the first and second harmonics for the cases where the second mode was observed. Also the bispectral analysis did not show any coupling between the low frequency facility noise and the second mode.

Model pressure distributions were measured in all of the experiments (Lachowicz, Doggett and Blanchard) and examples are shown for the Doggett case in Figures 28 and 29. Figure 28 is for the zero angle of attack case and the distribution is seen to closely match computational predictions using the Navier-Stokes CFL3D code (see references 18 or 19 for details). The installation uncertainty in the angle of attack of +/- 0.2 degrees which could not account for the small devaition between the measurements and theory at the higher Reynolds numbers possibly due to the transitional flow in that region. Figure 29 shows the pressure distribution for the 2 degree case. Again, the correspondence between computation and experiment appear to be quite good.

Discussion

The studies reviewed in this paper are the first stability experiments conducted in a facility designed specifically for high-Reynolds-number, low-disturbance free-stream flow. As such, the facility should be as much an object of scrutiny as the model experiments. Discussion therefore will highlight the facility-related aspects of the studies where relevant.

For the cases of combined adiabatic-wall/adverse-pressure-gradient and cold-wall/adverse-pressure-gradient, the e^N method (as implemented in reference 7) was able to predict both the frequency and integrated growth rate of the most amplified disturbances (See Figure 11) . Stability computations were not available for the angle-of-attack study. For the case of the flow on the windward side of the model, however, where the second mode was still clearly evident, similar favorable results would not be unexpected. The reason for the success of the linear theory must be attributed to the low free-stream disturbance quality of the wind tunnel and the inclusion of the relevant physics in the computation of the mean flow.

It was noted with regard to the tunnel that two noise fields were of interest - the high intensity intermittency or turbulence associated with turbulent breakdown in the nozzle wall boundary layer and a lower-level, low-frequency disturbance field preceding the intermittency. The later field is apparently due to growing nozzle wall instabilities, presumably the Görtler mode in this case. In these experiments, the models were completely free from the high intensity noise but were subjected to the lower level noise over the aft portion of each model. In all

cases, the receptivity-sensitive nose region of the models were free from both noise sources. As evidenced by the excellent correspondence between linear theory and the experimental data, the radiated forcing of the aft portions of the models apparently had minimal impact on transition. This is similar to the case of the Langley Mach 3.5 Supersonic Low Disturbance Tunnel in which the aft portions of the model were subjected to the turbulent radiated nozzle wall noise but were still able to match linear theory[30]. In terms of hypersonic quiet tunnel technology, it appears that it will be difficult to get away from the situation where some amount of radiated noise is directed at the aft portion of the model as long as the tunnel is required to be used at its maximum quiet Reynolds number in order to achieve transition on the model. In the Langley 18 Inch Mach 8 Quiet Tunnel (18M8QT) currently being readied for flow quality testing, it would not be surprising to find a similar state of affairs. The 18M8QT was designed with the same features as the M6NTC (slotted throat, axisymmetric, slow expansion nozzle) as the Mach 6 nozzle.

In terms of general comparisons between the current experiments and those conducted in AEDC VKF Tunnel B (reference 3) at Mach 6 and 8, the major differences appear to be due to be higher and more uniform free stream noise amplitude in Tunnel B rather than any fundamental instability process differences. The general features of the second mode instability growth process in both tunnels appear to be the same. For example the boundary layer spectra of reference 3 for a Mach 8 sharp cone qualitatively closely resemble Figure 10, 17 or 19 for the current experiments at Mach 6 with pressure gradient. The reason is that both are dominated by the second mode. The main differences in correspondence to linear theory is apparently related to the initial disturbance amplitude. Figure 27 reproduced from reference 3 shows the free stream noise spectra for several unit Reynolds numbers in the Tunnel B Mach 8 nozzle on the centerline. A trend of increasing free stream spectral amplitude and bandwidth is evident. This is to be compared to Figure 13 for the M6NTC taken outside the boundary layer of the 91-6 flared cone at a single unit Reynolds number. In Tunnel B, in the case of, say, the seven degree sharp cone, with a second mode frequency of approximately 100 kHz, there is a measurable free stream disturbance across the free stream bandwidth affecting the entire model, especially the sensitive nose region. For the M6NTC model 91-6 with a second mode frequency of approximately 300 kHz, there is no measurable free stream disturbance energy affecting any portion of the nose region of the model and only frequencies much lower than the second mode affecting the aft portion of the model. Absence of a measurable hot wire signal is not synonymous, however, with an absence of low level seed energy for the second mode. A disturbance generated either in the stream or on the model, however small must ultimately supply the seed energy for the instability.

As a final point, all of the experiments discussed thus far have been for simple geometries with a single region below the neutral curve or a single receptivity-sensitive region. In this case, it has been suggested that is not surprising that the AEDC Tunnel B work and that in the LaRC M6NTC share many qualitative similarities. If multiple receptivity regions were involved however on a model with a more complicated configuration, the case might well be different. The possibility of multiple instability modes merging and interacting downstream could show significant free stream disturbance sensitivity.

Summary

This paper has reviewed three previously published low free stream disturbance stability studies and a facility study that were conducted in the final 14 months of operation of the Langley Mach 6 Quiet Nozzle in the Nozzle Test Chamber (M6NTC). Stability modifiers including adverse pressure, wall cooling, angle of attack and nose bluntness were investigated. The experiments included a detailed study of mean flow and stationary free-stream-disturbance patterns in the Mach 6 nozzle. They also included stability experiments on 18 inch and 20 inch long cone-flare models at a unit Reynolds number sufficient to capture most of the transition zone under low-disturbance free stream conditions. The experiments documented the growth of the second mode for the cases of: approximately constant adverse pressure gradient; small stabilizing nose bluntness; wall cooling; and angle of attack. The base configuration for each of the experiments was the cone-flare.

The results showed that the M6NTC was nominally quiet up to a unit Reynolds number 2.8 million/ft. Two noise patterns were found in the freestream corresponding to instability growth on the nozzle wall followed by itermittency and turbulence. All model experiments were conducted with more than one half of the model free from any measurable free stream disturbances and with only the aft portion subjected to low-frequency, low-level rms disturbances from the instability process on the nozzle wall. In no case was the model ever subjected to intermittency or turbulence from the nozzle wall.

Transition on the models was consistent with previous findings in hypersonic flow: adverse pressure gradient, wall cooling and angle-of-attack on the leeward side destabilized the boundary layer; small nose bluntness and angle-of-attack on the windward side stabilized the boundary layer. Stability measurements showed in all cases (except small bluntness which was virtually completely stabilizing) that transition was dominated by the second mode with some evidence that the Görtler mode may have been operative as well. Furthermore, comparisons with linear stability theory show excellent agreement with both predicted second mode frequency and integrated growth rate. Second mode saturation occurred at N factors in the range of 8.5 to 11.

Acknowledgments

The author gratefully thanks Drs. Alan E. Blanchard, Glen P. Doggett, Jason T. Lachowicz, and Ndaona Chokani for their exceptional efforts in obtaining and analyzing the data reviewed in this report and for their helpful comments on the manuscript. Their work was supported under NASA Cooperative Agreements NCC-1-180 and NCC-1-183.

References

[1] Wilkinson S.P., Anders S.G., Chen F.-J. and Beckwith I.E.: Supersonic and Hypersonic Quiet Tunnel Technology at NASA Langley, AIAA Paper 92-3908, July, 1992.

[2] Wilkinson S.P., Anders S.G., Chen F.-J. and White J.A.: Status of NASA Langley Quiet Flow Facility Developments, AIAA Paper 94-2498, June, 1994.

[3] Stetson, K.F. and Kimmel R.L.: On Hypersonic Boundary-Layer Stability, AIAA Paper 92-0737, Jan. 1992.

[4] Kimmel, R.L.: Experimental Transition Zone Lengths in Pressure Gradient in Hypersonic Flow, in ASME FED Vol. 151, Transitional and Turbulent Compressible Flows, 1993, pp 117-127.

[5] Malik, M.R., Balakumar P. and Chang, C.-L.: Effect of Adverse Pressure Gradient on the Second Mode Instability in Hypersonic Boundary Layers, High Technology Corporation, Hampton, VA, Report No. HTC-9006, December, 1990.

[6] Malik, M.R.: e^{Malik}: A New Spatial Stability Analysis Program for Transition Prediction Using the e^N Method. High Technology Corporation, Hampton, VA, Report No. HTC-9203, 1992.

[7] Balakumar P. and Malik M.R.: Effect of Adverse Pressure Gradient and Wall Cooling on Instability of Hypersonic Boundary Layers, High Technology Corporation, Hampton, VA, Report No. HTC-9404, March, 1994.

[8] Pruett C.D. and Chang C.-L.: Spatial Direct Numerical Simulation of High-Speed Boundary-layer Flows - Part II: Transition on a Cone in Mach 8 Flow, Theoretical and Computational Fluid Dynamics, Vol. 7, No. 5, 1995, pp 397-423.

[9] Chen F.-J., Wilkinson S.P. and Beckwith I.E.: Gortler Instability and Hypersonic Quiet Nozzle Design, AIAA Journal of Spacecraft and Rockets, Vol 30 , No. 2, March-April 1993, pp 170-175.

[10] Blanchard A.E., Lachowicz J.T. and Wilkinson S.P.: NASA Langley Mach 6 Quiet Wind- Tunnel Performance, AIAA Journal, Vol. 35, No. 1, January, 1997, pp 23-28.

[11] Blanchard A.E., Lachowicz J.T. and Wilkinson S.P.: Performance of the NASA-Langley Mach 6 Quiet Wind Tunnel, AIAA Paper 96-0441, January, 1995.

[12] Lachowicz J.T., Chokani N. and Wilkinson S.P.: Boundary-Layer Stability Measurements in a Hypersonic Quiet Tunnel, AIAA Journal, Vol. 34, No. 12, December, 1996, pp 2496-2500.

[13] Lachowicz J.T., Chokani N. and Wilkinson S.P.: Hypersonic Boundary layer Stability over a Flared Cone in a Quiet Tunnel, AIAA Paper 96-0782. January, 1996.

[14] Lachowicz J.T., Hypersonic Boundary Layer Stability Experiments in a Quiet Wind Tunnel with Bluntness Effects, Ph.D. Dissertation, Mechanical and Aerospace Engineering Dept., North Carolina State University, Raleigh, NC, November 1995.

[15] Lachowicz J.T. and Chokani N.: Hypersonic Boundary Layer Stability Experiments in a Quiet Wind Tunnel with Bluntness Effects, NASA CR-198272, January, 1996.

[16] Doggett, G.P., Chokani N. and Wilkinson S.P.: Effect of Angel of Attack on Hypersonic Boundary-Layer Stability, AIAA Journal, Vol. 35, No. 3, March, 1997, pp.464-470.

[17] Doggett G.P., Chokani N. and Wilkinson S.P.: Hypersonic Boundary-Layer Stability Experiments on a Flared-Cone Model at Angle of Attack in a Quiet Wind Tunnel, AIAA Paper 97-0557, January, 1997.

[18] Doggett G.P., Hypersonic Boundary-Layer Stability on a Flared-Cone Model at Angle of Attack, Ph.D. Dissertation, Mechanical and Aerospace Engineering Dept., North Carolina State University, Raleigh, NC, May 1996.

[19] Doggett G.P. and Chokani N.: Hypersonic Boundary-Layer Stability Experiments on a Flared-Cone Model at Angle of Attack in a Quiet Wind Tunnel, NASA CR 201617, October 1996.

[20] Blanchard A.E.: An Investigation of Wall-Cooling Effects on Hypersonic Boundary-Layer Stability in a Quiet Wind Tunnel, Ph.D. Dissertation, Old Dominion University, Dept. of Mechanical Engineering, Norfolk, VA, December, 1995

[21] Blanchard A.E. and Selby, G.V.: An Experimental Investigation of Wall-Cooling Effects on Hypersonic Boundary-Layer Stability in a Quiet Wind Tunnel, NASA CR-198287, February, 1996.

[22] Cavalieri, D.: "On the Experimental Design for Instability Analysis on a Cone at Mach 3.5 and 6 Using a Corona Discharge Perturbation Method", M.S. Thesis, Illinois Inst. of Tech. 1995.

[23] Pruett C.D. and Chang C.-L.: Direct Numerical Simulation of Hypersonic Boundary-Layer Flow on a Flared Cone, Journal of Theoretical and Computational Fluid Dynamics (submitted for publication)

[24] Mangalam S.M., Sarma G.R., Kuppa S. and Kubendran L.R.: A New Approach to High Speed Flow Measurements Using Constant Voltage Anemometer, AIAA Paper 92-3957, 1992.

[25] Sarma, G.R.: Analysis of a Constant Voltage Anemometer Circuit, IEEE/IMTC Conference, Irvine, CA, May, 1993.

[26] Kegerise M.A.: A Study of the Constant-Voltage Hot-Wire Anemometer, MS Thesis, Syracuse University, December, 1196.

[27] Kegerise M.A. and Spina E.F.: A Comparative Study of Constant-Voltage and Constant-Temperature Hot-Wire Anemometers in Supersonic Flow, ASME FED, Vol. 239, 1996, pp. 297-308

[28] Mack L.M.: Linear Stability Theory and the Problem of Supersonic Boundary-Layer Transition, AIAA Journal Vol. 13, No. 3, March, 1975, pp278-289.

[29]Kendall, J.M.: Wind Tunnel Experiments Relating to Supersonic and Hypersonic Boundary-Layer Transition, AIAA Journal Vol. 13, No. 3, 1975, pp. 290-299

[30] Chen F.-J., Malik M.R. and Beckwith I.E.: Comparison of Boundary Layer Transition on a Cone and Flat Plate at Mach 3.5, AIAA Paper 88-0411, January, 1988.

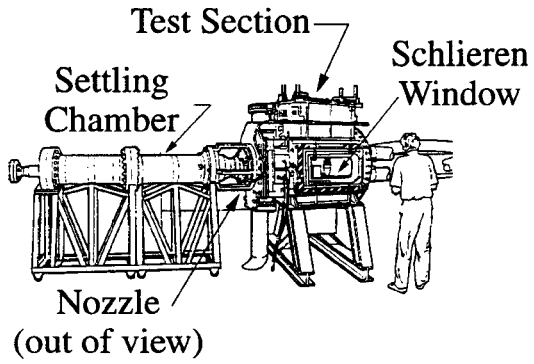

Figure 1. Nozzle Test Chamber with Mach 6 Quiet Nozzle

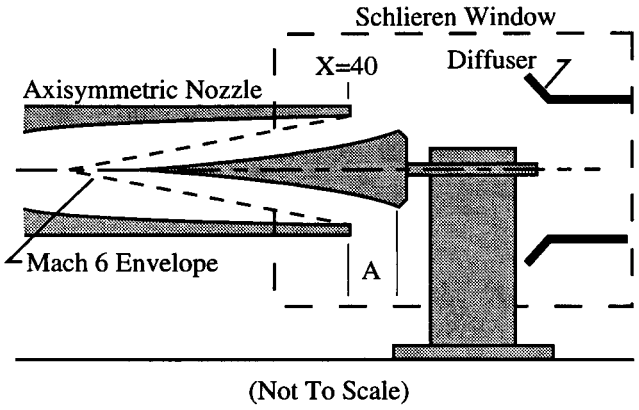

Figure 2. Placement of Flared-Cone Models in M6NTC. A= 3 inch (Model 91-6), 3.5 in. (Model 93-10)

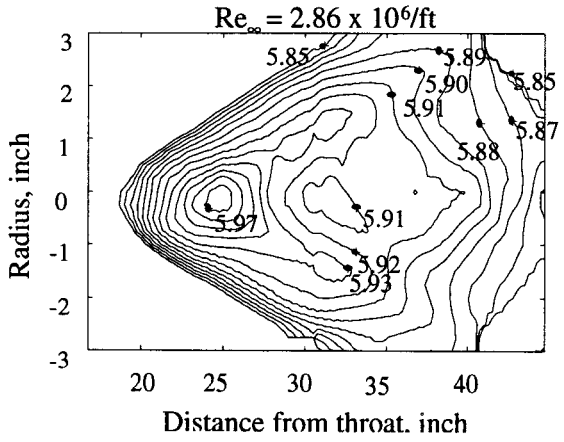

Figure 3. Contour Plot of Mean Mach Number on Nozzle Horizontal Center Plane

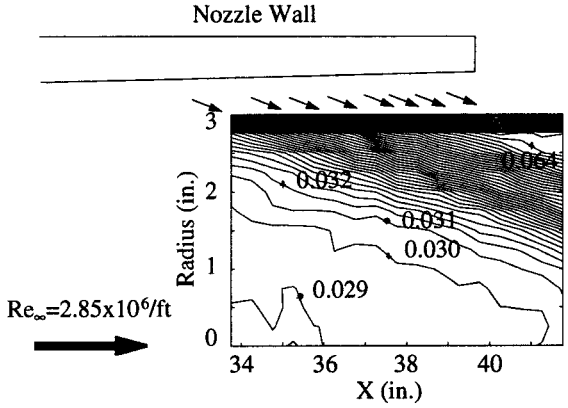

Figure 4. Contour Plot of RMS Fluctuations on Nozzle Horizontal Center Plane

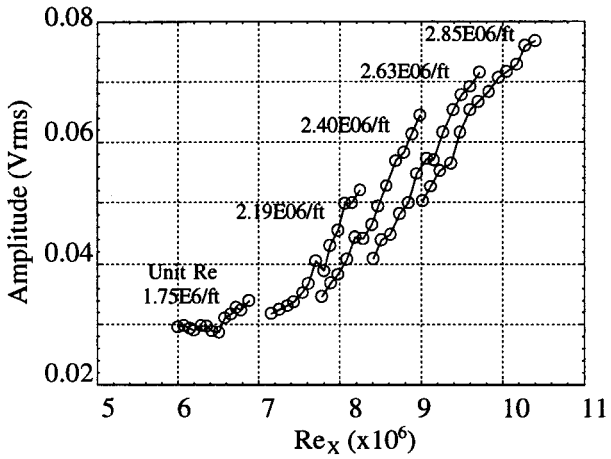

Figure 5. Growth of RMS Fluctuations on Nozzle Centerline at Various Unit Reynolds Numbers

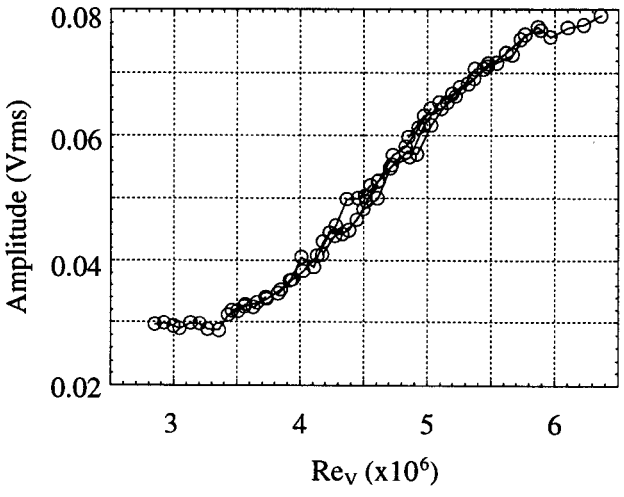

Figure 6. Figure 5 Re-plotted Based on Virtual Origin Location, V=X-14.76 inch.

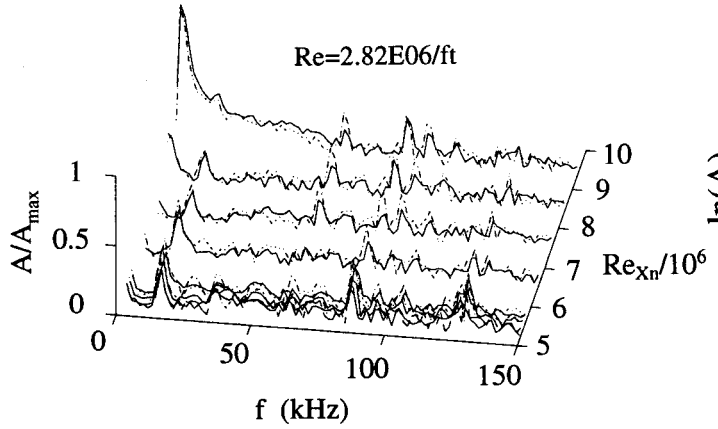

Figure 7. Freestream Noise Spectra (solid: y=1.25 in. ; dotted: y=-1.25 in.)

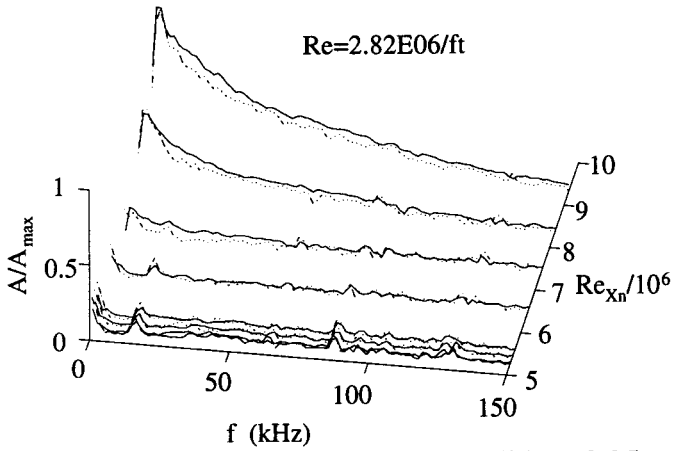

Figure 8. Freestream Noise Spectra (solid: y=2.25 in.; dotted: y=-2.25 in.)

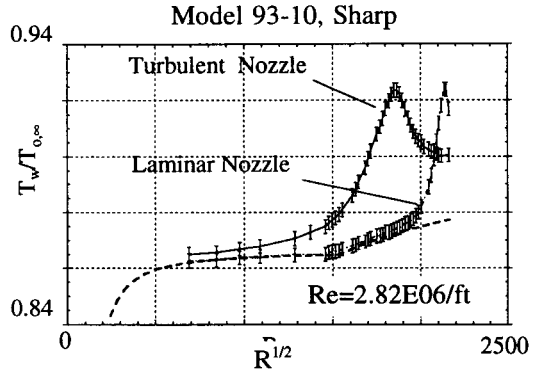

Figure 9. Surface Temperature Distribution for Quiet and Noisy Nozzle Flow (dashed: theory)

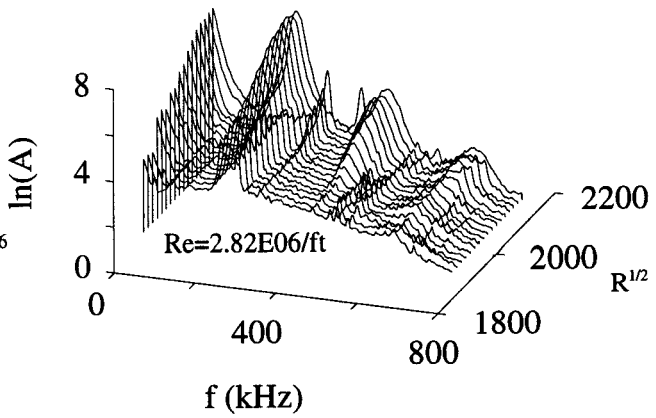

Figure 10. Fluctuation Spectra for Model 93-10 (Sharp) at Maximum Energy Location

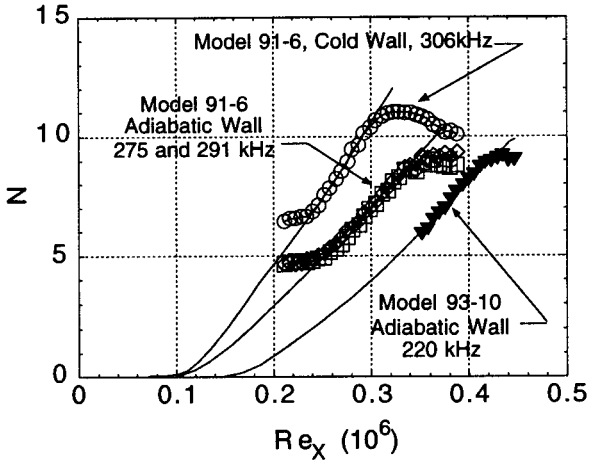

Figure 11. N-Factor Distributions for All Models Tested. Unit Re = 2.83E06/ft.

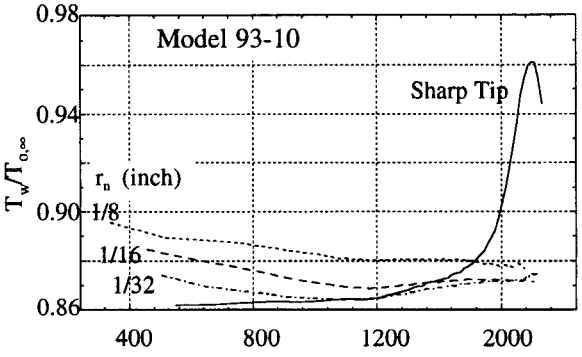

Figure 12. Surface Temperature Distributions for Small Bluntness Radii

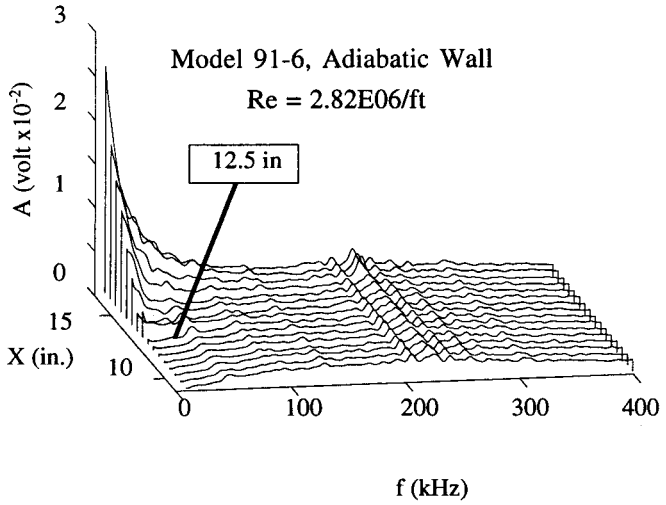

Figure 13. Freestream Noise Spectra Between Boundary Layer Edge and Shock

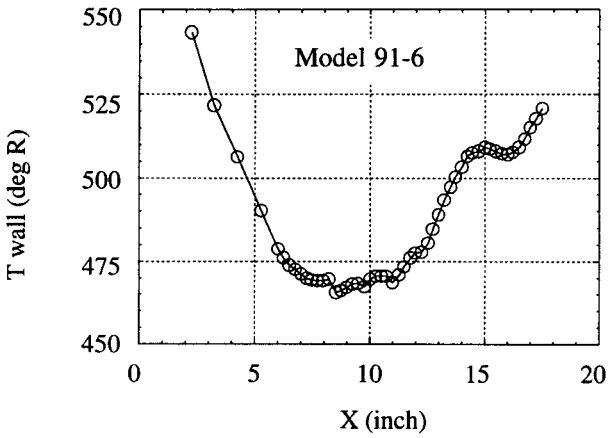

Figure 14. Wall Temperature Distribution, Cold Wall Case

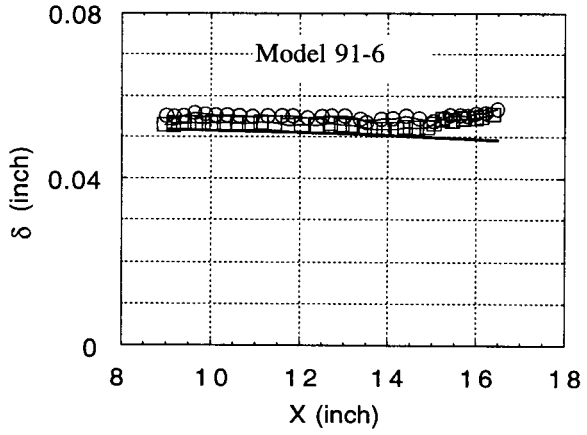

Figure 15. Boundary Layer Thickness, Adiabatic Wall (circle: wire resistance, square: mean voltage, line: theory)

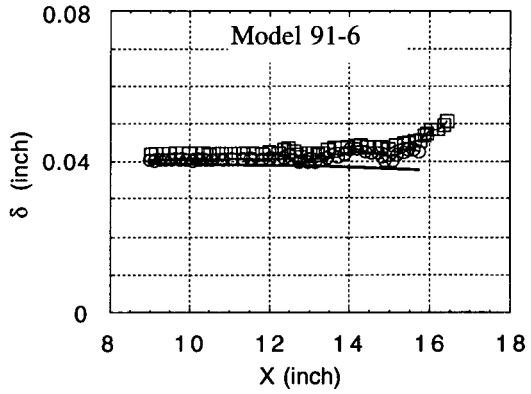

Figure 16. Boundary Layer Thickness, Cold Wall (circle: wire resistance, square: mean voltage, line: theory)

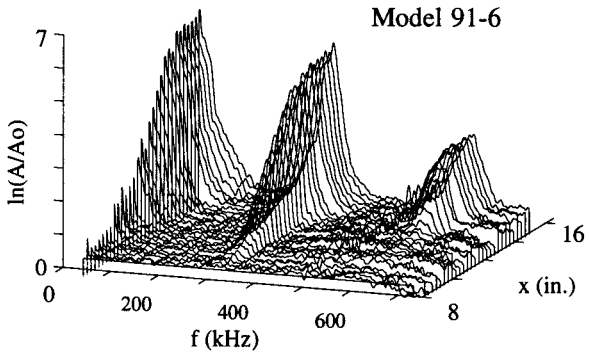

Figure 17. Fluctuation Spectra at Maximum Energy Location, Adiabatic Wall (Perspective View)

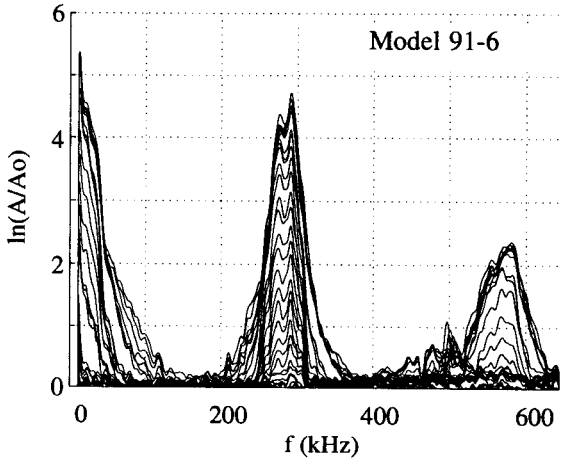

Figure 18. Fluctuation Spectra at Maximum Energy Location, Adiabatic Wall (Frontal View)

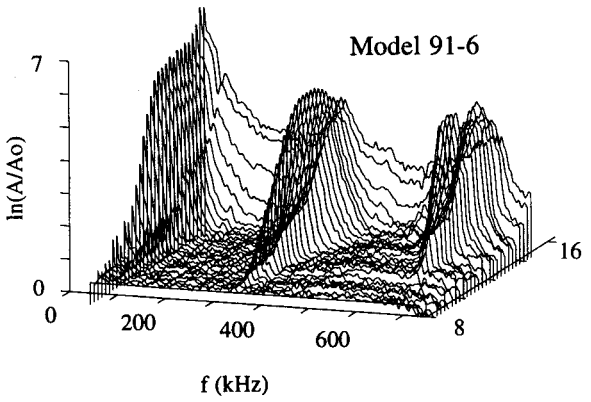

Figure 19. Fluctuation Spectra at Maximum Energy Location, Cold Wall (Perspective View)

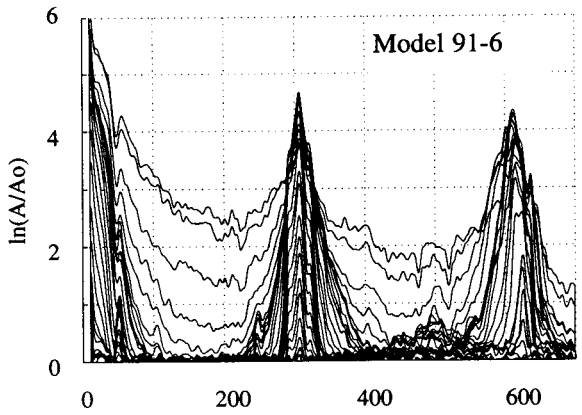

Figure 20. Fluctuation Spectra at Maximum Energy Location, Cold Wall (Frontal View)

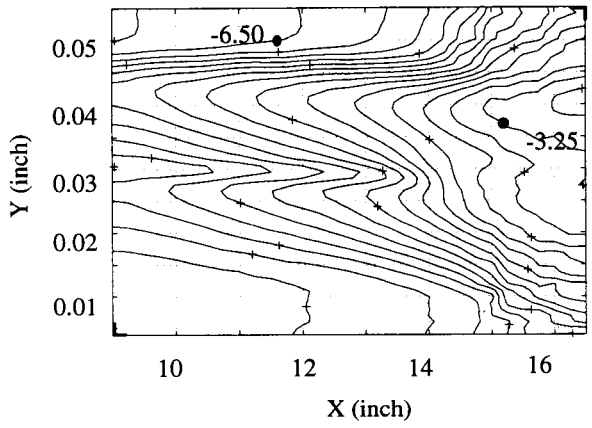

Figure 21. Contour plot of normalized boundary layer fluctation amplitude (ln(A/Aref), rms), Model 91-6, adiabatic wall, contour increment 0.25, monotonically increasing from left to right

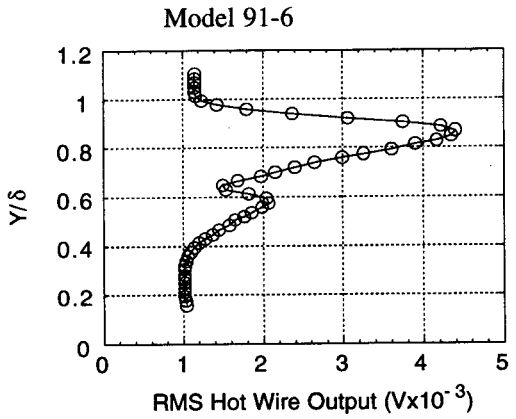

Figure 22. RMS Hot Wire Fluctuation Voltage Through Boundary Layer, Adiabatic Wall

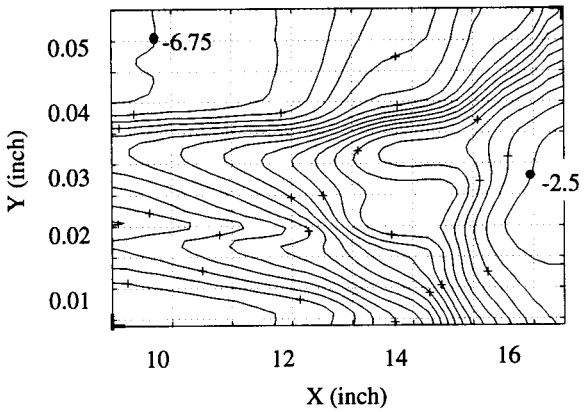

Figure 23. Contour plot of normalized boundary layer fluctation amplitude (ln(A/Aref), rms), Model 91-6, cold wall, contour increment 0.25, monotonically increasing from left to right

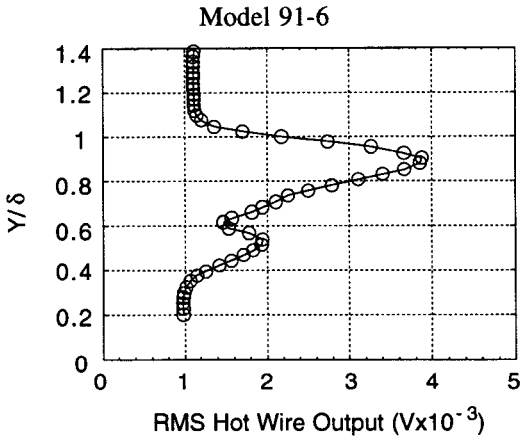

Figure 24. RMS Hot Wire Fluctuation Voltage Through Boundary Layer, Cold Wall

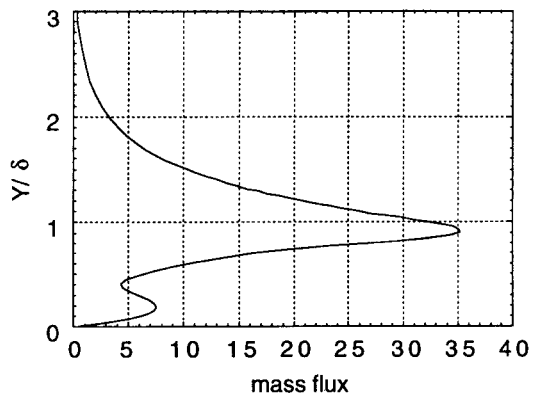

Figure 25. Computed RMS eigenfunction for Model 93-6. f=310kHz, T_{wall}= 420 deg R, X=9 inch, P_0=130 psia.

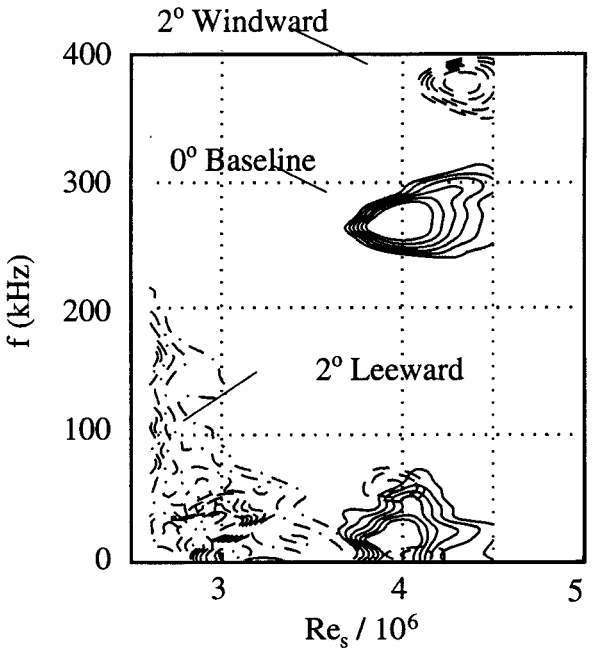

Figure 27. Partial stability diagram for angle of attack studies.

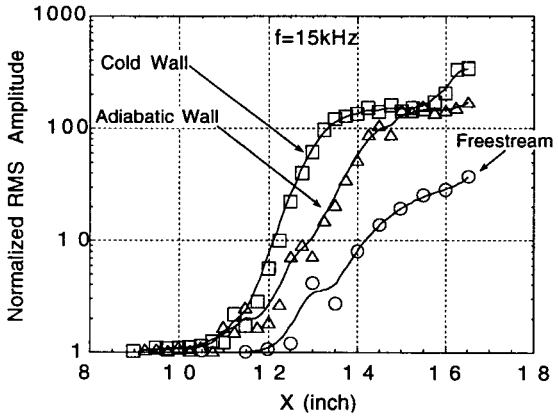

Figure 26. Low Frequency Disturbance Growth (f= 15 kHz) Following Maximum Energy Location

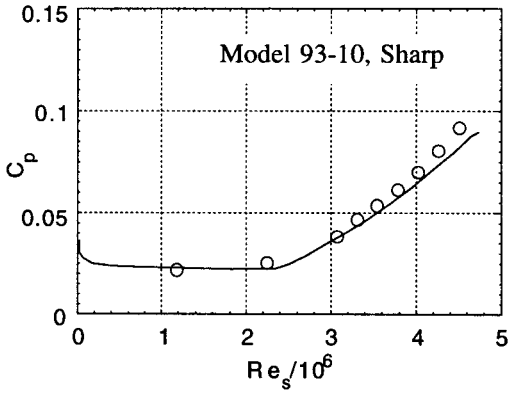

Figure 28. Surface Pressure Coefficient, α=0 degree

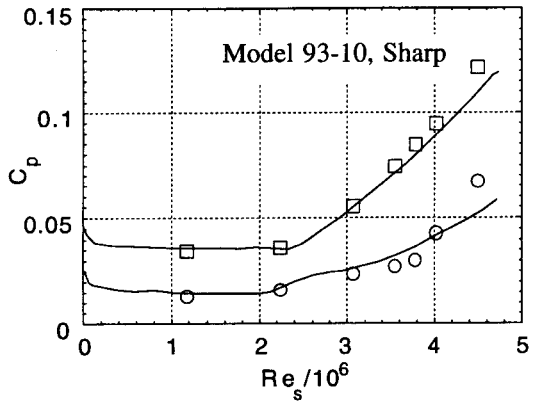

Figure 29. Surface Pressure Coefficient, α=+/- 2 degree

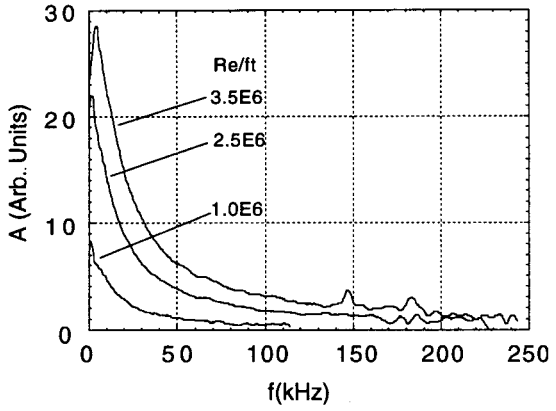

Figure 30. Tunnel Freestream Noise, AEDC VKF Tunnel B, Mach 8 (from ref. 1)